

The Relation of Neutron Incommensurability to Electronic Structure in High Temperature Superconductors

M. R. Norman

Materials Science Division, Argonne National Laboratory, Argonne, IL 60439

The relation between the incommensurability observed in neutron scattering experiments in bilayer cuprate superconductors and the electronic structure is investigated. It is found that the observed incommensurability pattern, as well as its dependence on energy, can be well reproduced by electronic dispersions motivated by angle resolved photoemission data. The commensurate resonance and its contribution to the superconducting condensation energy are discussed in the context of these calculations.

PACS numbers: 25.40.Fg, 71.25.Hc, 74.25.Jb, 74.72.Hs

I. INTRODUCTION

One of the more controversial topics in the field of high temperature cuprate superconductivity is the origin of the incommensurability observed by neutron scattering experiments. The original explanation of this phenomenon was that it was due to Fermi surface nesting¹. Later, it was proposed that it was due to the formation of stripes². These two explanations are so different, one would expect that ways of differentiating them using existing data should be possible. In bilayer cuprates, the situation is even more interesting, in that a commensurate resonance is seen, along with incommensurability at energies off resonance^{3,4}.

In this paper, the Fermi surface nesting approach is analyzed based on tight binding energy dispersions motivated by angle resolved photoemission spectroscopy (ARPES) studies, with the dynamic susceptibility calculated using the random phase approximation (RPA). Such tight binding dispersions are able to reproduce the commensurate resonance, along with the incommensurability off resonance. In particular, the incommensurability wavevector is found to be energy dependent, in good agreement with recent experimental results⁴. This would seem to argue against a stripes interpretation, where one would expect the incommensurability to be energy independent. Moreover, the incommensurability in the RPA calculations is very sensitive to the underlying electronic structure, which has implications for the position and curvature of the Fermi surface near the d-wave node. As for the commensurate resonance, it is a more robust feature of these calculations, though its width in momentum space is sensitive to the location of the flat band near $(\pi, 0)$. In support of earlier estimates⁵⁻⁷, the change in exchange energy between the normal and superconducting states in these calculations is sufficient to account for the superconducting condensation energy.

In Section II, the details of the computations are given. In Section III, the commensurate resonance is discussed in relation to the electronic structure, with Section IV dealing with the same relation in regards to the incommensurability off resonance. Section V uses these cal-

culations to comment on the question of the lowering of the exchange energy in the superconducting state. Some conclusions are offered in Section VI.

II. CALCULATIONAL DETAILS

The methodology used here is essentially the same as that of other groups⁸⁻¹¹. The only difference is to use energy dispersions motivated by actual fits to photoemission measurements. As in these earlier studies, one first determines the non-interacting susceptibility, which in the superconducting state is composed of three terms^{12,9}:

$$\begin{aligned} \chi_0(q, \omega) = & \sum_k \left\{ \frac{1}{2} \left(1 + \frac{\epsilon_k \epsilon_{k+q} + \Delta_k \Delta_{k+q}}{E_k E_{k+q}} \right) \frac{f(E_{k+q}) - f(E_k)}{\omega - (E_{k+q} - E_k) + i\delta} \right. \\ & + \frac{1}{4} \left(1 - \frac{\epsilon_k \epsilon_{k+q} + \Delta_k \Delta_{k+q}}{E_k E_{k+q}} \right) \frac{1 - f(E_{k+q}) - f(E_k)}{\omega + (E_{k+q} + E_k) + i\delta} \\ & \left. + \frac{1}{4} \left(1 - \frac{\epsilon_k \epsilon_{k+q} + \Delta_k \Delta_{k+q}}{E_k E_{k+q}} \right) \frac{f(E_{k+q}) + f(E_k) - 1}{\omega - (E_{k+q} + E_k) + i\delta} \right\} \quad (1) \end{aligned}$$

where ϵ_k is the dispersion, Δ_k the superconducting gap, E_k the quasiparticle energies ($\sqrt{\epsilon_k^2 + \Delta_k^2}$), and f the Fermi function. The three terms are due to quasiparticle scattering, quasiparticle pair annihilation, and quasiparticle pair creation, respectively. At low temperatures, only the last process contributes. Note this equation makes a severe approximation of treating the single particle spectral function as a delta function. On the other hand, at low temperatures, photoemission data indicate quasiparticle peaks at all \mathbf{k} vectors near the Fermi surface¹³ (though along the d-wave node direction, there is still some controversy¹⁴). As the incoherent part of the spectral function is unlikely to lead to sharp structure in \mathbf{q} and ω , these earlier studies based on Eq. 1 are followed, but the reader should keep in mind that there are certainly quantitative, and perhaps qualitative, differences between this “quasiparticle” susceptibility and the true one which warrant future investigation.

To evaluate Eq. 1, $i\delta$ is replaced by $i\Gamma$ in the energy denominators. The resulting well behaved function is

then summed over a 400 by 400 mesh in the Brillouin zone. Γ , which is a crude representation of broadening due to interactions and disorder, was taken to be 2.4 meV. Smaller values of Γ simply lead to sharper structure in χ_0 which requires a denser \mathbf{k} mesh in the sum.

The interacting susceptibility in the RPA is given by

$$\chi(q, \omega) = \frac{\chi_0(q, \omega)}{1 - J(q)\chi_0(q, \omega)} \quad (2)$$

where $J(q)$ is the spin-spin response function. Many studies set $J(q)$ to a constant, J , but in several treatments^{8,11}, $J(q)$ is assumed to be of the form $J_q = -J(\cos(q_x a) + \cos(q_y a))/2$ due to superexchange between near-neighbor Cu sites, so calculations were performed with both $J(q) = J$ and $J(q) = J_q$. The use of J_q tends to suppress incommensurability since J_q is largest at the commensurate wavevector (π, π) .

For energy dispersions, a number of model dispersions present in the literature^{15,16,11,17} were analyzed. These are based on tight binding functions, and in the more sophisticated models designed to fit photoemission data, they contain an expansion up to a real space lattice vector of $(2,2)$ ¹⁵⁻¹⁷. The first to be considered is one¹⁶ which does a very good job of modeling the normal state ARPES dispersion in $Bi_2Sr_2CaCu_2O_8$ (Bi2212)¹⁸. This is reproduced in Table I. Note that this model dispersion has no bilayer splitting, consistent with its lack of experimental observation in Bi2212¹⁸. J is then chosen to yield a resonance at a particular energy. A d-wave energy gap is assumed of the form $\Delta_k = \Delta(\cos(k_x) - \cos(k_y))/2$. An s-wave gap strongly reduces the tendency to obtain a commensurate resonance because of the BCS coherence factors in Eq. 1^{19,20}.

III. COMMENSURATE RESONANCE

The first question addressed concerns the commensurate resonance, first observed in $YBa_2Cu_3O_7$ (YBCO)^{21,22,20,23}, and recently in Bi2212^{24,25}. The conditions under which a commensurate response is obtained for the non-interacting susceptibility in a simple t, t' tight binding model is given in Ref. 10, and are roughly obeyed for the more sophisticated dispersions considered here. For simplicity, consider first the normal state. Then, the condition reduces to whether the Fermi surface is centered at $(0,0)$ or at (π, π) . In the former case, the response becomes incommensurate, basically because the Fermi surface and its shadow image, displaced by a wavevector (π, π) , no longer intersect (the intersection points are referred to as hot spots in the literature). Once a superconducting gap opens, there is a correction to this condition which scales like Δ ²¹⁰. For the dispersion analyzed here, this correction corresponds to about 5 meV. That is, once the band at $(\pi, 0)$ becomes more than 5 meV above the Fermi energy, the response becomes completely incommensurate. All models for YBCO, and most

models for Bi2212, are in favor of Fermi surfaces centered about (π, π) . An exception is a recent model by Chuang *et al* for Bi2212²⁶. In this model, the Fermi crossing is far enough away from $(\pi, 0)$ along the $(0, 0) - (\pi, 0)$ line that an incommensurate response is expected, unlike what is observed experimentally²⁴.

The non-interacting susceptibility having its maximum response at (π, π) leads to a maximum at (π, π) in the interacting susceptibility as well. For a d-wave gap, the coherence factors in Eq. 1 are maximal on the Fermi surface, due the sign change of the gap under (π, π) translation. This leads to an abrupt rise in $\text{Im}\chi_0$ above some threshold energy value (twice the superconducting energy gap at the hot spots), which is not present for the s-wave case. By Kramers-Kronig transformation, the abrupt rise causes a peak in $\text{Re}\chi_0$ ²⁷. Therefore, if J is large enough, a zero will occur in the real part of the denominator of Eq. 2 for energies smaller than the threshold. As $\text{Im}\chi_0$ is small below the threshold, this leads to a resonance like behavior in $\text{Im}\chi$. That is, in general, one expects a resonance at a energy smaller than $2\Delta_{max}$. These points are illustrated in Fig. 1. Note that all the peak structures in this plot become more pronounced if the broadening, Γ , is reduced in size.

An interesting evolution of this resonance occurs as the chemical potential, μ , is varied. Using the same model dispersion, J was adjusted for each μ in such a way that the maximum in $\text{Im}\chi$ occurs at 39 meV (with Δ_{max} taken to be 35 meV). In Fig. 2, a 2D contour plot is shown at the resonance energy for various positions of the band at $(\pi, 0)$, $\epsilon(\pi, 0)$. As $\epsilon(\pi, 0)$ approaches μ from below, the resonance broadens in momentum space, and eventually transforms from a circular pattern to a square-like pattern. As the band crosses μ , the resonance pattern rotates to a diamond shape, and then far enough beyond, a completely incommensurate response is achieved. In agreement with the analytic results on the t, t' model for $\text{Im}\chi_0$ ¹⁰, the value of $\epsilon(\pi, 0)$ relative to μ where the crossover to incommensurate behavior occurs is found to be proportional to Δ^2 . The width of the resonance in momentum space is also sensitive to other factors. The above calculations assumed $J(q) = J$. If $J(q) = J_q$ is used instead, the resonance would become narrower in q , which is obvious from the q dependence of J_q , J_q being maximal at (π, π) . Also, the dispersion used in the above calculation is based on normal state ARPES data. In the superconducting state, though, it is known that the dispersion becomes flatter near $(\pi, 0)$ ²⁸, which acts to broaden the resonance in momentum space. From experiment, the resonance in Bi2212 is broader in momentum space than in YBCO²⁵. In the context here, this would imply that for Bi2212 relative to YBCO: (1) the band at $(\pi, 0)$ is closer to the chemical potential, (2) the dispersion at $(\pi, 0)$ is flatter, and/or (3) $J(q)$ is flatter near (π, π) . A quantitative comparison of experiment to theory will be discussed in Section V.

At this stage, nothing has been said about the q_z dependence of the resonance. Experimentally, the reso-

nance only appears in the odd ($q_z = \pi$) channel. There are three ways this could occur in the context of the RPA calculations. First, $J(q)$ could be larger in the odd channel than the even one due to interplane exchange⁸. In this case, the pronounced gap in the even channel would be associated with the threshold energy discussed earlier for $\text{Im}\chi_0$ (twice the energy gap at the hot spots). Although experimentally, $J(q)$ is larger in the odd channel²⁹, the value of the interplane exchange integral (J_\perp) is small enough that there would be qualitative problems with fitting the even channel data. For instance, for both dispersions listed in Table I, given a value of J needed to obtain a resonance at 39 meV in the odd channel, a 20% reduction in J to simulate the even channel still results in a pronounced resonance. An exception is the dispersion of Ref. 17, where the same analysis leads to no resonance in the even channel. This occurs because the peak in $\text{Re}\chi_0$ in Fig. 1 is very shallow. For the same reason, though, a value of J much larger than experiment is needed (~ 1 eV) to obtain a resonance in the odd channel.

The second way would be to recognize that the odd channel corresponds to connecting bonding to antibonding states in Eq. 1, whereas the even channel connects bonding to bonding and antibonding to antibonding⁹. In this context, bonding and antibonding refer to the bilayer splitting of the electronic structure. As mentioned above, there is little evidence for such splitting from ARPES data in Bi2212, even in the superconducting state¹⁸ (although recently, this result has been challenged³⁰). Still, several calculations including bilayer splitting were analyzed. In the first case, dispersion two in Table I was taken to be the bonding band, and the antibonding dispersion was gotten by adding a constant in such a way that its Fermi surface crossing occurred along the $(0, 0) - (\pi, 0)$ line. In the second case, the bilayer split dispersion of Ref. 17 was used. In the first case, there was virtually no change in the results. In the second case, there were some minor quantitative differences (i.e., a pronounced resonance still existed in the even channel). It should be remarked that although the evidence for bilayer splitting is considerably greater in YBCO¹⁷, the interpretation of ARPES data in this case is more controversial due to the contribution from the chains, as well as surface related problems.

The third possibility is that the $\langle \Delta_k \Delta_{k+Q} \rangle$ correlator in Eq. 1 only contributes to the odd channel for some reason not apparent at the moment³¹. In this regard, it is interesting to note that Janko³² has recently predicted, based on thermodynamic arguments, that the resonance will be strongly suppressed for fields along the c-axis. As Janko discusses, the likely source of this field dependence is that the $\langle \Delta_k \Delta_{k+Q} \rangle$ correlator in Eq. 1 is sensitive to phase coherence. This has also been suggested to be the case in the context of interpreting c-axis optical conductivity measurements³³. This same phase coherence sensitivity might be linked to why the resonance only appears in the odd channel.

IV. INCOMMENSURATE RESPONSE

The next question concerns the incommensurate behavior off resonance. Only in YBCO is this known in detail^{3,4}. Incommensurate behavior is observed in Bi2212 as well²⁴, but the 2D pattern of this in q space, as well as its energy dependence, is unknown at this time. Interestingly, in YBCO, the incommensurate wavevector depends on energy⁴. It basically has an “hourglass” shape, with the incommensurability wavevector approaching the commensurate value as the resonance is approached from below, then again splitting out above the resonance energy. In the RPA calculations, although incommensurability above the resonance energy is a robust result, being related to the commensurate/incommensurate discussion of the previous Section, the incommensurability below the resonance energy is a different matter altogether. Incommensurability below resonance has been present in previous calculations³⁴, and the explanation for it within the RPA context was given in a recent paper by Brinckmann and Lee¹¹, with the calculations presented here in agreement with their picture. In the superconducting state, the constant energy contours at low energies are very elongated due to the large ratio of the Fermi velocity at the d-wave node to the slope of the superconducting energy gap at the node. This velocity ratio has been experimentally determined by ARPES to be 20 for Bi2212³⁵, and the same value has been extracted from low temperature thermal conductivity measurements³⁶. The latter measurements have also determined the velocity ratio to be 14 in YBCO. As shown by Brinckmann and Lee¹¹, the incommensurability is due to nesting between the energy contour about the d-wave node to the same contour displaced by a wavevector $Q = (\pi, \pi)$, that is, $E_k \sim \omega/2$, $E_{k+Q} \sim \omega/2$, where ω is the neutron energy. The wavevector is incommensurate since the Fermi surface at the node is displaced away from the $(\pi/2, \pi/2)$ points.

For the dispersion used in Fig. 2, though, no incommensurability is found below the resonance energy, though incommensurability does occur above the resonance energy. This can be traced to the fact that for this dispersion, the Fermi surface is too curved at the node. This leads to low energy contours which have a “banana” shape, thus destroying nesting, as illustrated in Fig. 3. Moreover, for this dispersion, the Fermi crossing at the d-wave node corresponds to a wavevector of $(0.37, 0.37)\pi$, which would yield a larger incommensurability than is typically observed. Both of these problems can be corrected if the Fermi wavevector is pushed closer to the $(\pi/2, \pi/2)$ point. This has the effect of reducing the Fermi surface curvature, thus enhancing nesting, and also reducing the magnitude of the incommensurability. Reducing the Fermi velocity also aids the nesting, but this is a smaller effect.

To investigate these points further, several modifications to the dispersion used in Fig. 2¹⁶ were made. First,

the very flat dispersion of the superconducting quasiparticle states near $(\pi, 0)$ was incorporated by setting $\epsilon(\pi, 0)$ to -5 meV, and then invoking the condition that the curvature of ϵ_k is zero along the k_x and k_y axes at this point. To obtain an incommensurability more relevant to experimental data, the Fermi wavevector at the node was pushed out to $(0.41, 0.41)\pi$. At the same time, the Fermi velocity was reduced from 1.6 eVÅ to 1.0 eVÅ, but as discussed above, this has a smaller influence on the results. This dispersion (two) is also listed in Table I, with the resulting Fermi surface and low energy contours shown in Fig. 3 as well. Note the flatter energy contours as compared to the previous dispersion.

In Fig. 4 (left panels), 2D contour plots are shown for this dispersion at three different energies: on resonance, and 10 meV above and below resonance. Note that the incommensurability pattern below resonance has a striking “baseball diamond” shape, very similar to what has been observed experimentally in YBCO³. This pattern was generated assuming $J(q) = J$. If $J(q) = J_q$ is used instead (right panels), another maximum develops at the commensurate wavevector, and is or is not the global maximum depending on the particular energy. In this context, a number of model dispersions were analyzed. Some exhibit completely commensurate behavior below resonance, others completely incommensurate behavior, and others still mixed behavior. That is, in the RPA context, the incommensurability below resonance is very sensitive to the electronic structure, as well as to the momentum dependence of $J(q)$.

In Fig. 5 (left panel), the wavevector along the (π, π) direction where $\text{Im}\chi$ is maximal is plotted versus energy, using the same parameters as Fig. 4. Note the distinct “hourglass” shape of the pattern, which has recently been observed experimentally in YBCO⁴. The striking agreement of this pattern with experiment is a strong argument in favor of an RPA-like interpretation of the data. On the other hand, the RPA calculations do suffer from some quantitative problems. In the right panel of Fig. 5, the intensity at the wavevector where $\text{Im}\chi$ is maximal is plotted versus energy. Note the extremely sharp drop as one moves off resonance. Experimentally, this drop is less pronounced³.

As suggested above, in the RPA context, the neutron scattering results are a sensitive probe of the electronic structure. This raises the question of whether the incommensurability structure is in quantitative agreement with ARPES results or not. Unfortunately, all neutron scattering studies on this issue but one have been done on YBCO. ARPES results on YBCO are still somewhat controversial because of surface related issues not present in Bi2212. For instance, the tight binding dispersions proposed in Ref. 17 do not support incommensurate behavior below the resonance energy, again because of too strong a curvature of the Fermi surface around the node (that is, the low energy contours are too curved to support nesting). Moreover, published ARPES results on YBCO indicate a Fermi crossing along the node which

would result in an incommensurate wavevector which is too far displaced from (π, π) relative to experiment. It would, of course, be desirable in YBCO to exploit the advent of the Scienta high momentum resolution detectors to revisit this issue.

In Bi2212, the ARPES Fermi surface (in the vicinity of the d-wave node, at least) is better agreed upon. As for neutron results, only one study has been offered²⁴. In that experiment, a rod of crystallites aligned along the $(1, 1)$ direction was measured. This indicated an incommensurate wavevector at low temperatures of around $(0.82, 0.82)\pi$. Note that the two dimensional pattern of the structure is not known from these data. Moreover, energy information is also not known, so there is always the possibility that the incommensurability being observed is above resonance. Lacking further data at this stage, let us assume that incommensurability is indeed being observed below resonance. Then, for the ARPES data to be consistent with the neutron wavevector, the Fermi crossing along the node would have to be at about $(0.40, 0.40)\pi$. This is close to a recently reported value of $(0.39, 0.39)\pi$ using a Scienta detector¹⁴. So, the reported wavevectors from the ARPES and neutron experiments are certainly within current error bars, and therefore consistent at this stage. It would be highly desirable to: (1) have neutron data on the incommensurability on single crystal samples of Bi2212, and (2) to have more accurate measurements of both the Fermi wavevector, and the curvature of the Fermi surface around the node, from ARPES data, to further explore this point.

V. SUM RULE AND CONDENSATION ENERGY

Finally, the intriguing question of the relation of the commensurate resonance to the superconducting condensation energy can be treated very straightforwardly in the RPA context. The advantage of these calculations is that all wavevectors and energies are accounted for, and therefore these calculations provide an important check to the ideas proposed in Refs. 5 and 6.

To begin with, χ has to be converted to units quoted in neutron scattering work. This is achieved by multiplying Eq. 2 by the appropriate matrix element. For simplicity, consider the zz matrix element, which is $\sum_{\sigma} g^2 \mu_B^2 \langle \sigma | S_z | \sigma \rangle^2$. For $g = 2$, $S = 1/2$, this reduces to $2\mu_B^2$, as do the other two (xx , yy). The sum rule³⁷ can now be checked by summing Eq. 2 over the zone, integrating ω out to the band edges, and multiplying by $2\mu_B^2$. The dispersion used in Fig. 5 is employed here, with a resonance at 39 meV obtained by setting J to 159 meV, a value comparable to experimental estimates of J in YBCO²⁹. The normal state is calculated by simply setting Δ to zero. This is a gross approximation, since it assumes quasiparticle states at $T=0$ for the normal state, which is highly improbable. In principle, a more accurate representation of the normal state could be simulated by

increasing Γ , but for simplicity, this is not done here. For $J(q) = J_q$, the sum is $1.62\mu_B^2$ in the normal state, $1.64\mu_B^2$ in the superconducting state. For $J(q) = J$, the sum is $1.93\mu_B^2$ in the normal state, $1.87\mu_B^2$ in the superconducting state. So, to within a few percent, the sum rule is satisfied by the RPA calculations. For a local moment system, we would expect the value $\pi g^2 \mu_B^2 S(S+1)/3^{29,23}$, which for $g = 2$, $S = 1/2$ reduces to π . That is, the above values range from 52% to 61% of the local moment result. This reduction is to be expected, since Eq. 2 is based on itinerant electrons.

A useful comparison to experiment is to integrate $\text{Im}\chi(\pi, \pi)$ over energy. Restricting to a 50 meV energy range, a value of $1.9\mu_B^2$ per plane is calculated, compared to an experimental value of $0.95\mu_B^2$ in Bi2212 and $0.8\mu_B^2$ in YBCO²⁵. This somewhat large overshoot³⁸ is reduced when looking at the local susceptibility (q integrated). The maximum (at the resonance energy) per plane from the above calculation is $9.8\mu_B^2/\text{eV}$ for $J(q) = J_q$, $14.9\mu_B^2/\text{eV}$ for $J(q) = J$. This is comparable to the $9.5\mu_B^2/\text{eV}$ value quoted for underdoped YBCO³. 10 meV below resonance, the numbers are 1.1 and 2.2, respectively, compared to an experimental value of 2.5³. As noted in the previous Section, for any given calculation, the intensity appears to drop off below resonance faster than experiment. Another useful comparison is to look at the full width half maximum of the resonance in q space. The calculated values are 0.34\AA^{-1} for $J(q) = J$, 0.23\AA^{-1} for $J(q) = J_q$. This is to be compared to experimental values of 0.52\AA^{-1} for Bi2212 and 0.25\AA^{-1} for YBCO²⁵.

As noted in earlier work⁵⁻⁷, the exchange energy contribution to the free energy in the t-J model, denoted as E_X , is obtained by multiplying $\text{Im}\chi$ as defined in Eqs. 1 and 2 by $-3J_q/2\pi$, integrating over energy, and summing over the zone. Its contribution to the condensation energy is $E_X^{NS} - E_X^{SC}$, where NS represents an extrapolation of the normal state to zero temperature. For the case considered above, a value per plane of 28K is found if $J(q) = J_q$ is used, 59K if $J(q) = J$. That is, within the t-J model context, the exchange energy is indeed lowered in the superconducting state, with the calculated values somewhat larger than those based on the data^{6,7}. The advantage of the current calculation is that this difference can be looked at as a function of q and ω . In Fig. 6a, the zone sum of $J_q \text{Im}\chi_q$ is plotted as a function of ω ($J(q) = J$) for normal and superconducting states. Note that the two merge at $2\Delta_{max}$, that is, the energy difference is confined to energies below this. In Fig. 6b, the ω integrated quantity is plotted versus q . Note the contribution near (π, π) due to the resonance. In addition, a normal state contribution at low q is removed in the superconducting state. If $J(q) = J_q$ is used instead (Fig. 6d), the low q structure in the normal state is suppressed, which is why the condensation energy is half that of the $J(q) = J$ case. This additional low q structure is likely not relevant to experiment since there

is no evidence for it, and it is doubtful whether the true $J(q)$ is large at small wavevectors.

The implications of Fig. 6 is clear. The dominant contribution to the exchange energy part of the condensation energy is due to the resonance. This in support of previous work^{6,7}. Moreover, as noted before^{6,7}, the estimated value, such as from the above calculation, is more than sufficient to account for experiment, as the total condensation energy has been estimated to be only 3K per copper oxide plane from specific heat data for optimal doped YBCO³⁹. (It should be mentioned that within the t-J context, if the exchange energy is lowered in the superconducting state, then it is expected that the kinetic energy would increase⁴⁰.) It is also interesting to remark that the RPA calculations appear to be in greater agreement with the idea of Ref. 6 (that the resonance dominates the exchange energy difference) than related calculations based on the spin-fermion model⁴¹, despite qualitatively similar physics. In the latter model, the merger noted in connection with Fig. 6a occurs at much higher energies (of order J).

Finally, some comments in regards to the nature of the resonance mode are in order. The quantum numbers of the resonance correspond to an excited triplet ($S = 1$) pair with center-of-mass momentum $Q = (\pi, \pi)$, since the BCS ground state is $S = 0$, $Q = 0$, and the resonance is seen by spin flip scattering. On the other hand, the question of whether the mode is actually a particle-particle mode is a more delicate question, due to particle-hole mixing in the superconducting state⁴². The RPA calculation assumes that the underlying action is in the particle-hole channel. Is there any experimental support for this? As Demler and Zhang point out⁴², this question can only be indirectly answered by neutron scattering, as the neutrons only couple to the particle-hole channel. Their argument is that since the resonance only appears below T_c , and since particle-hole mixing occurs below T_c , then a particle-particle mode would only become visible in neutron scattering below T_c , in agreement with experiment. Of course, in the RPA calculations presented here, the mode also appears only in the superconducting state, since it is a consequence of the BCS coherence factors in Eq. 1 (that is, the mode is best not thought of as just a spin-wave mode). Now, although it is true that a spectral gap opens up above T_c in underdoped materials (the pseudogap), the RPA calculations are based on quasiparticle states, which only appear below T_c ⁴³. So, in that sense, the Demler-Zhang argument does not necessarily resolve this issue.

On the other hand, angle resolved photoemission does not have the same restriction as neutron scattering. Strong arguments have been made that the dramatic change in the spectral lineshape observed in such data below T_c are a direct consequence of the interaction of the electrons with the resonance mode^{28,44,27}. This comes from the dressing of the electron propagator by the resonance. Note that unlike neutrons, there is nothing restricting this coupling to be in the particle-hole chan-

nel. That is, one expects that if the mode were particle-particle in nature, the dominant coupling to the self-energy of the electrons would be in the particle-particle channel. Let us now think about the simple limit that the mode energy goes to zero. Then, the dispersion of the higher binding energy feature seen in ARPES data (the so-called hump) will have a dispersion given by solving a very simple 2 by 2 secular equation⁴⁵. In the particle-hole case, the diagonal elements will be ϵ_k and ϵ_{k+Q} , where $Q = (\pi, \pi)$. In the particle-particle case, the second element would become $-\epsilon_{-k+Q}$ instead. To first approximation in both cases, the off-diagonal elements, denoted as Δ_U , are taken to be constants. In Fig. 7, the dispersions obtained from both secular equations are plotted using dispersion one of Table I for ϵ_k , for a typical value of Δ_U (100 meV). For the particle-hole case, the resulting dispersion is very similar to what is observed in photoemission^{46,44}. But, the particle-particle case has no resemblance at all to the data.

Now, this argument does not definitively rule out a particle-particle explanation for the mode, since it is conceivable that the dominant coupling of the mode to the electrons could still be in the particle-hole channel because of the interaction vertices. Still, the above argument is certainly very suggestive of a particle-hole origin for the mode, and would also more naturally explain how the higher binding energy feature crosses over to the Mott insulating gap as the doping is reduced^{46,47,44}.

VI. CONCLUSIONS

In summary, this paper has shown that the RPA treatment of the dynamic susceptibility gives very useful insight into neutron scattering data in the cuprate superconductors. In such a framework, the neutron data are a sensitive probe of the underlying electronic structure. Using dispersions motivated by angle resolved photoemission data, a natural explanation is found for the magnetic resonance observed by neutrons, as well as the incommensurability seen off resonance. Moreover, these calculations are in support of previous suggestions^{6,7} that the resonance mode provides the dominant contribution to the change in the exchange energy between the normal and superconducting states. The advantage of the RPA calculations is that they provide quantitative information on all of these issues. In particular, the current study suggests that the two momentum resolved probes used for the cuprates, ARPES and neutrons, are strongly related to one another, and are consistent within current experimental error bars. With the advent of higher momentum resolution detectors in ARPES, and large enough samples for neutron studies, this connection in the future can be studied with much greater precision, especially in the case of Bi2212.

ACKNOWLEDGMENTS

The author would like to thank Herb Mook for suggesting this project. He would also like to thank Juan Carlos Campuzano, Helen Fretwell, and Adam Kaminski for discussions concerning photoemission data. This work was supported by the U.S. Dept. of Energy, Basic Energy Sciences, under Contract No. W-31-109-ENG-38.

-
- ¹ Q. Si, Y. Zha, K. Levin, and J. P. Lu, Phys. Rev. B **47**, 9055 (1993); P. Benard, L. Chen, and A.-M. S. Tremblay, Phys. Rev. B **47**, 15217 (1993); P. B. Littlewood, J. Zaanen, G. Aeppli, and H. Monien, Phys. Rev. B **48**, 487 (1993).
 - ² J. M. Tranquada, *et al.*, Nature **375**, 561 (1995).
 - ³ H. A. Mook, *et al.*, Nature **395**, 580 (1998).
 - ⁴ M. Arai, *et al.*, Phys. Rev. Lett. **83**, 608 (1999).
 - ⁵ D. J. Scalapino and S. R. White, Phys. Rev. B **58**, 8222 (1998).
 - ⁶ E. Demler and S.-C. Zhang, Nature **396**, 733 (1998).
 - ⁷ P. Dai, *et al.*, Science **284**, 1344 (1999).
 - ⁸ D. Z. Liu, Y. Zha, and K. Levin, Phys. Rev. Lett. **75**, 4130 (1995).
 - ⁹ N. Bulut and D. J. Scalapino, Phys. Rev. B **53**, 5149 (1996).
 - ¹⁰ M. Lavagna and G. Stemmman, Phys. Rev. B **49**, 4235 (1994).
 - ¹¹ J. Brinckmann and P. A. Lee, Phys. Rev. Lett. **82**, 2915 (1999).
 - ¹² J. R. Schrieffer, *Theory of Superconductivity* (Benjamin/Cummings, Reading, 1964).
 - ¹³ A. Kaminski, *et al.*, preprint cond-mat/9904390.
 - ¹⁴ T. Valla, *et al.*, Science **285**, 2110 (1999).
 - ¹⁵ R. J. Radtke and M. R. Norman, Phys. Rev. B **50**, 9554 (1994).
 - ¹⁶ M. R. Norman, M. Randeria, H. Ding, and J. C. Campuzano, Phys. Rev. B **52**, 615 (1995).
 - ¹⁷ M. C. Schabel, *et al.*, Phys. Rev. B **57**, 6090 (1998).
 - ¹⁸ H. Ding, *et al.*, Phys. Rev. Lett. **76**, 1533 (1996).
 - ¹⁹ P. Monthoux and D. J. Scalapino, Phys. Rev. Lett. **72**, 1874 (1994).
 - ²⁰ H. F. Fong, *et al.*, Phys. Rev. Lett. **75**, 316 (1995).
 - ²¹ J. Rossat-Mignod, *et al.*, Physica C **185-189**, 86 (1991).
 - ²² H. A. Mook, *et al.*, Phys. Rev. Lett. **70**, 3490 (1993).
 - ²³ H. F. Fong, *et al.*, preprint cond-mat/9910041.
 - ²⁴ H. A. Mook, F. Dogan, and B. C. Chakoumakos, preprint cond-mat/9811100.
 - ²⁵ H. F. Fong, *et al.*, Nature **398**, 588 (1999).
 - ²⁶ Y.-D. Chuang, *et al.*, Phys. Rev. Lett. **83**, 3717 (1999).
 - ²⁷ A. Abanov and A. V. Chubukov, Phys. Rev. Lett. **83**, 1652 (1999).
 - ²⁸ M. R. Norman, *et al.*, Phys. Rev. Lett. **79**, 3506 (1997); M. R. Norman and H. Ding, Phys. Rev. B **57**, R11089 (1998).
 - ²⁹ S. M. Hayden, *et al.*, Physica B **241-243**, 765 (1998).
 - ³⁰ D. L. Feng, *et al.*, preprint cond-mat/9908056.

- ³¹ P. W. Anderson, *The Theory of Superconductivity in the High T_c Cuprates* (Princeton Univ. Pr., Princeton, 1997).
- ³² B. Janko, preprint cond-mat/9912073.
- ³³ L. B. Ioffe and A. J. Millis, *Science* **285**, 1241 (1999).
- ³⁴ Y. Zha, K. Levin, and Q. M. Si, *Phys. Rev. B* **47**, 9124 (1993); Y.-J. Kao, Q. Si, and K. Levin, preprint cond-mat/9908302.
- ³⁵ J. Mesot, *et al.*, *Phys. Rev. Lett.* **83**, 840 (1999).
- ³⁶ M. Chiao, *et al.*, preprint cond-mat/9910367.
- ³⁷ Formally, it is the structure factor, S , which is involved rather than $\text{Im}\chi$, both for the sum rule and the condensation energy, but the difference is small.
- ³⁸ Similar overshoots have been reported in previous work; see D. K. Morr and D. Pines, *Phys. Rev. Lett.* **81**, 1086 (1998).
- ³⁹ J. W. Loram, K. A. Mirza, and P. F. Freeman, *Physica C* **171**, 243 (1990).
- ⁴⁰ For a very different perspective on this, see M. R. Norman, M. Randeria, B. Janko, and J. C. Campuzano, preprint cond-mat/9912043.
- ⁴¹ A. Abanov and A. V. Chubukov, preprint cond-mat/9909385.
- ⁴² E. Demler and S.-C. Zhang, *Phys. Rev. Lett.* **75**, 4126 (1995).
- ⁴³ M. R. Norman, M. Randeria, H. Ding, and J. C. Campuzano, *Phys. Rev. B* **57**, R11093 (1998).
- ⁴⁴ J. C. Campuzano, *et al.*, *Phys. Rev. Lett.* **83**, 3709 (1999).
- ⁴⁵ A. P. Kampf and J. R. Schrieffer, *Phys. Rev. B* **42**, 7967 (1990).
- ⁴⁶ D. S. Marshall, *et al.*, *Phys. Rev. Lett.* **76**, 4841 (1996).
- ⁴⁷ R. B. Laughlin, *Phys. Rev. Lett.* **79**, 1726 (1997).

TABLE I. Tight binding dispersions based on fitting ARPES data. The first two columns list the coefficient, c_i , of each term (eV), that is $\epsilon(\vec{k}) = \sum c_i \eta_i(\vec{k})$, with “one” a previous fit to normal state ARPES data¹⁶, and “two” a modified fit as discussed in the text. The last column lists the basis functions (the lattice constant a is set to unity).

one	two	$\eta_i(\vec{k})$
0.1305	0.0879	1
-0.5951	-0.5547	$\frac{1}{2}(\cos k_x + \cos k_y)$
0.1636	0.1327	$\cos k_x \cos k_y$
-0.0519	0.0132	$\frac{1}{2}(\cos 2k_x + \cos 2k_y)$
-0.1117	-0.1849	$\frac{1}{2}(\cos 2k_x \cos k_y + \cos k_x \cos 2k_y)$
0.0510	0.0265	$\cos 2k_x \cos 2k_y$

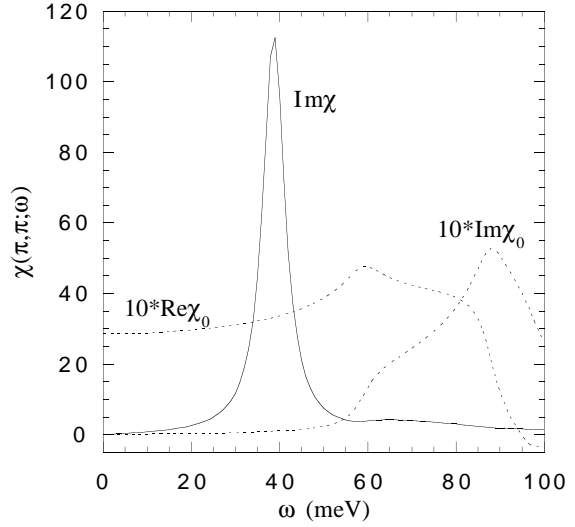


FIG. 1. $\text{Im}\chi_0$, $\text{Re}\chi_0$, and $\text{Im}\chi$ at $q = (\pi, \pi)$ using dispersion one listed in Table I, with $J=0.3$ eV, $\Gamma=2.4$ meV, $\Delta=35$ meV, and $T=13$ K. $\text{Im}\chi$ units (Eq. 1) are states/eV/CuO plane, which applies for all figures.

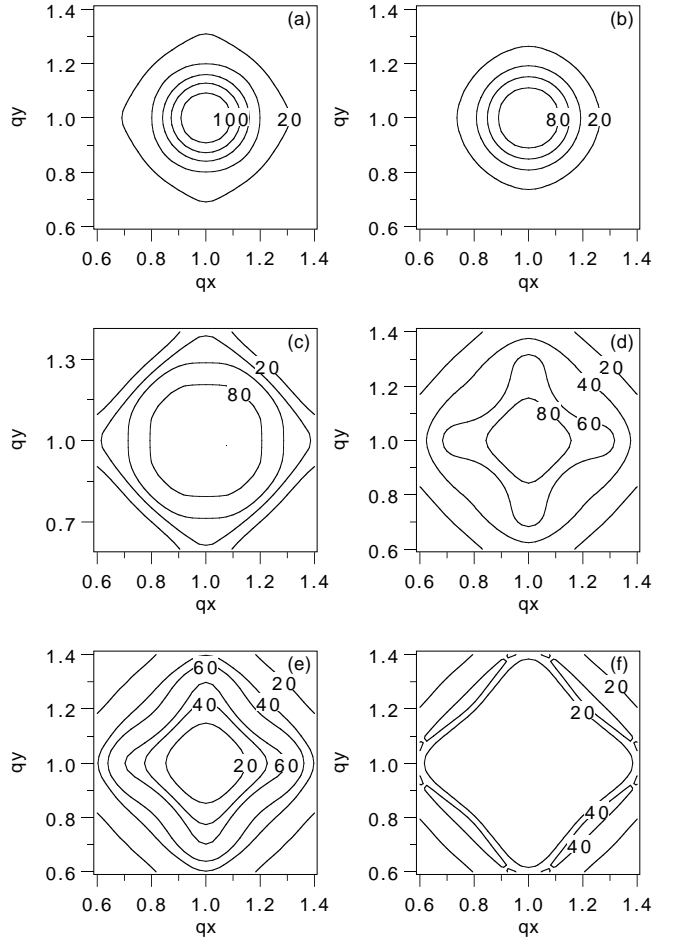


FIG. 2. Dependence of $\text{Im}\chi(q_x, q_y)$ at $\omega=39$ meV on $\epsilon(\pi, 0) - \mu$: (a) -34 meV, (b) -10 meV, (c) 0 meV, (d) +5 meV, (e) +10 meV, and (f) +20 meV (with (a) the value from dispersion one of Table I). Same parameters as Fig. 1, except that for each plot, $J(q) = J$ has been adjusted so that the maximum in $\text{Im}\chi$ is at this ω . Note that qx and qy are in units of π .

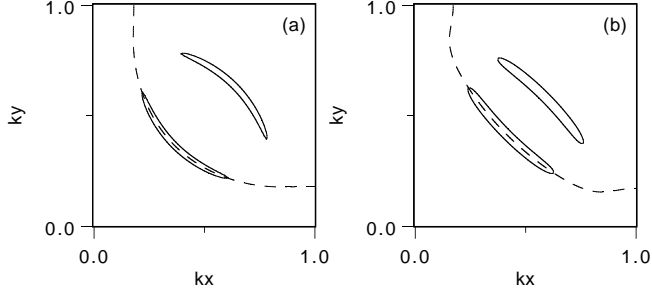


FIG. 3. Fermi surface (dashed curve) and superconducting state energy contours ($E_k, E_{k+Q} = \omega/2$, $\omega=29$ meV), for (a) dispersion one and (b) dispersion two in Table I. Note $Q = (1, 1)$ in these units.

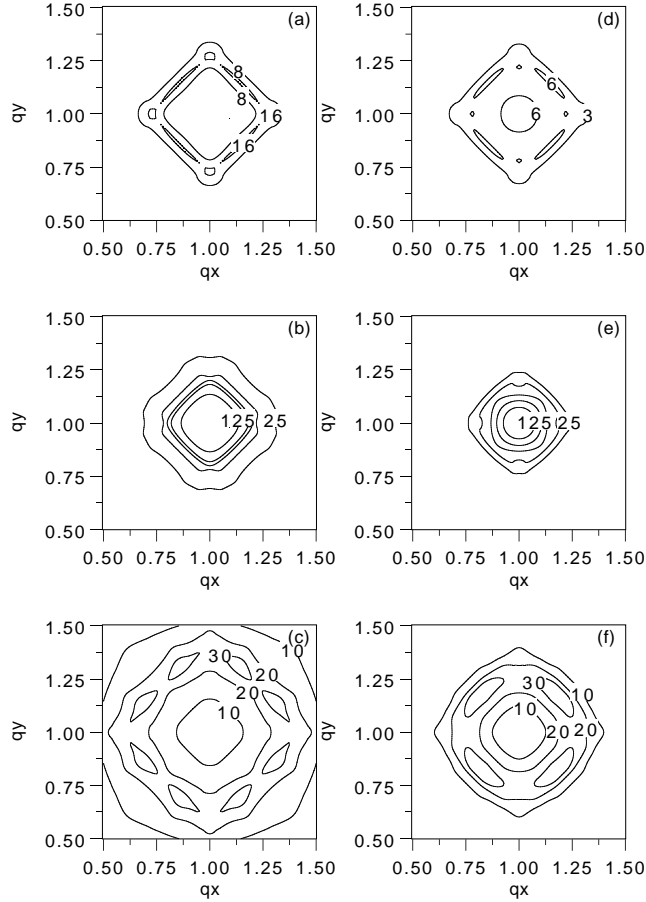


FIG. 4. $\text{Im}\chi(q_x, q_y)$ at three energies: (a) 29 meV, (b) 39 meV (resonance), and (c) 49 meV, for dispersion two of Table I, with $J=159$ meV ($J(q) = J$). (d), (e), and (f) are the same, but with $J(q) = J_q$.

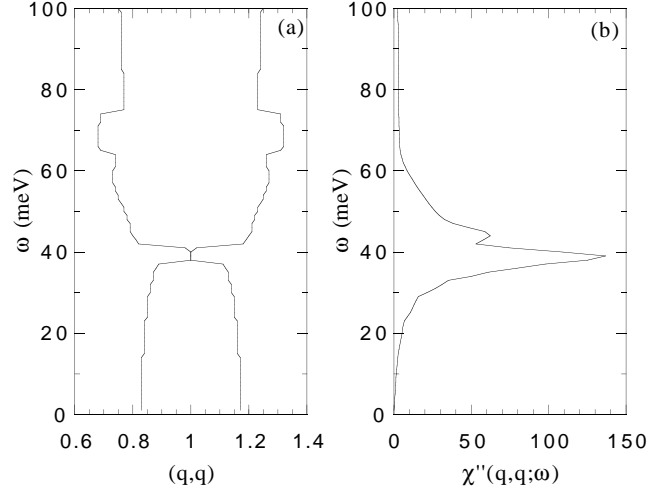


FIG. 5. (a) q vector along (π, π) direction where $\text{Im}\chi(q, q)$ is maximal versus ω . (b) The magnitude of $\text{Im}\chi$ in (a) versus ω . Same parameters as Fig. 4, with $J(q) = J$.

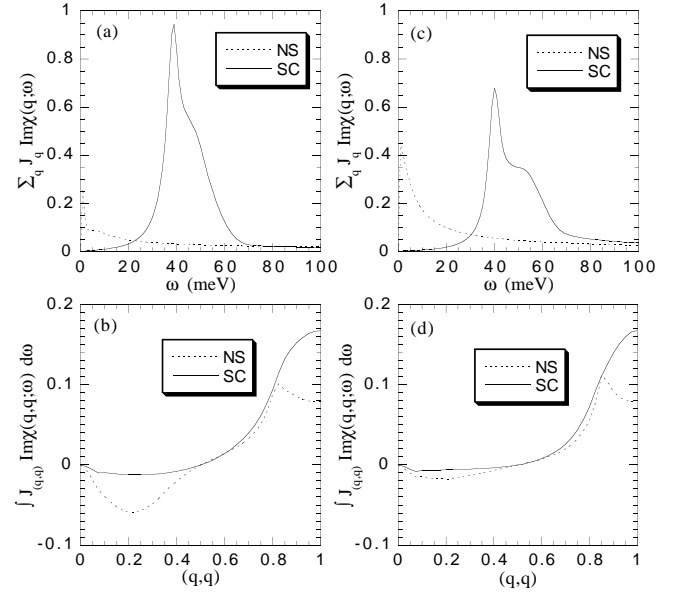


FIG. 6. (a) $\sum_q J_q \text{Im}\chi(q, \omega)$ and (b) $\int_0^{100\text{meV}} J_q \text{Im}\chi(q, \omega)$ for $J(q) = J$. Same parameters as in Fig. 5. (c) and (d) are the same, but with $J(q) = J_q$. NS is the normal state, SC the superconducting state. The exchange energy contribution to the condensation energy would be obtained by integrating (a) or (c) over ω , multiplying by $-3/(2\pi)$, and subtracting SC from NS. Note (b) and (d) are in eV units.

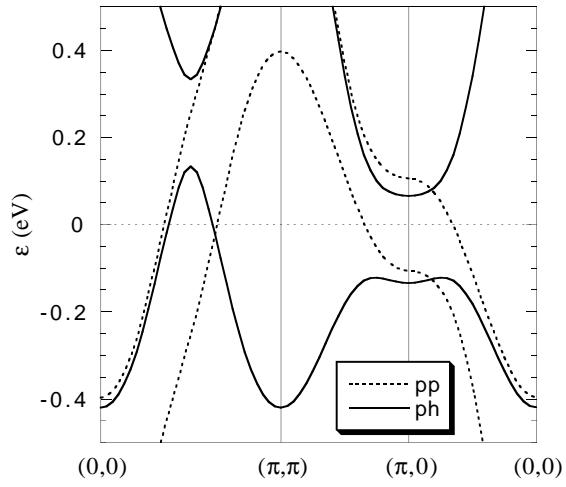


FIG. 7. Solution of particle-hole (ph) secular equation, with diagonal elements $\epsilon_k, \epsilon_{k+Q}$, and particle-particle (pp) secular equation, with diagonal elements $\epsilon_k, -\epsilon_{-k+Q}$, with $Q = (\pi, \pi)$. In both cases, the off-diagonal elements were taken to be $\Delta_U=100$ meV. Dispersion one of Table I was employed ($\mu=0$).